Microfluid Nanofluid (2013) 14:551–563
DOI 10.1007/s10404-012-1073-9

RESEARCH PAPER

Leukocyte enrichment based on a modified pinched flow fractionation approach

Claudio Cupelli · Thorsten Borchardt · Thomas Steiner · Nils Paust · Roland Zengerle · Mark Santer

Received: 16 April 2012 / Accepted: 14 August 2012 / Published online: 8 November 2012

Abstract In this paper, a simple and robust design for a passive hydrodynamic cell sorter based on pinched flow-field fractionation is presented and analyzed. Two principal layouts of the sorter are discussed and investigated experimentally as well as numerically based on the dissipative particle dynamics (DPD) method. Experimentally, design 1 approximately sorts 87 % of the erythrocytes to their designated outlet, while 100 % of the leukocytes branch correctly. This also holds for design 2 differing merely in the direction of the outlet for erythrocytes, but here only 69 % of the red blood cells are redirected to the designated outlet. This behavior can be elucidated by employing DPD simulations, where erythrocytes advected with the flow are modeled explicitly. Our results suggest that if a cell sorter is designed to operate at high throughput, its layout may not entirely rely on commonly assumed idealizing conditions, because cells cannot be considered as point-like, isolated objects following definite stream lines. Hydrodynamic forces originating from the cells as extended objects must be taken into account.

C. Cupelli · T. Borchardt · T. Steiner · R. Zengerle · M. Santer
Laboratory for MEMS Applications, Department of Microsystems Engineering (IMTEK), University of Freiburg, Georges-Koehler-Allee 103, 79110 Freiburg, Germany

N. Paust · R. Zengerle
HSG-IMIT, Institut für Mikro- und Informationstechnik, Georges-Koehler-Allee 103, 79110 Freiburg, Germany

R. Zengerle
Centre for Biological Studies (BIOSS), University of Freiburg, Georges-Köhler-Allee 106, 79110 Freiburg, Germany

M. Santer (✉)
Max Planck Institute of Colloids and Interfaces, 14424 Potsdam, Germany
e-mail: mark.santer@mpikg.mpg.de

Keywords Microfluidics · Cell sorting · Pinched flow fractionation · Micro total analysis systems · Dissipative particle dynamics

1 Introduction

The analysis of human blood for determining the health status of a patient is the aim of medical diagnostics. Table 1 gives an overview about the constituents of human blood (Riegger 2006).

While a large class of medical tests, e.g., immunoassays (Riegger 2006), rely on the analysis of the plasma and its suspended proteins, the number and size of specific blood particles itself, the so-called blood count, are an important indicators for the health status of a patient. Some diseases and the accompanying anomalies of the blood count are listed in Table 2. For instance, an increased value of lymphocytes above the physiological range of a healthy patient ($<0.3 \times 10^4$) cells per µl blood), can indicate lymphocytic leukemia.

In the past, the counting of blood cells was conducted manually by a medical technologist in a counting chamber with a specified volume of diluted blood. A difficulty encountered here is the rather poor statistics due to the strong variation in the total number of each cell type, e.g., the concentration of erythrocytes is approximately three orders of magnitudes higher than the leukocyte concentration (see Table 3). Therefore, the blood analysis has widely been automated by the so-called flow cytometry. These devices rely on a hydrodynamically focused stream (sheath flow) of blood cells, which are probed by a laser source. The absorbance and the scattering of the laser light are used to determine the size and also the type of cell. A tunable transducer permits the breaking of the sheath flow

Table 1 Blood constituents and the total volume fraction (TVF) within human whole blood (Riegger 2006)

Blood constituents	TVF (%)	RVF (%)
Plasma	45–65	
Water		90.2–92.2
Electrolytes		≈1
Proteins		6–8
Others		≈1
Cells	35–55	

The right column gives the relative volume fraction (RVF) within the plasma and serum, respectively

Table 2 Anomalies of the blood count as indicator for different diseases according to Riegger (2006)

Parameter	Increased value
Erythrocytes	Tolycythemia
Hematocrit	EPO doping
Neutrophils	Bacterial infection
Lymphocytes	Lymphocytic leukemia
Monocytes	Bacterial infection
Eosinophil	Parasitic infection

Table 3 Dimensions and concentration of erythrocytes and some selected leukocyte-cell types in human whole blood

Cell type	Cell size (μm)	Cells/μl
Erythrocytes	8 (width), 2 (height)	$4.4–5.5 \times 10^6$
Neutrophil	≈10–12	$0.26–0.72 \times 10^4$
Eosinophil	≈12−17	$0.16–0.44 \times 10^3$
Lymphocytes	≈7–8	$0.1–0.28 \times 10^4$

The shape of the leukocytes listed is a good approximation to a sphere (Young et al. 2006)

into single droplets, each of which contains a single cell (Howard 2003). After charging these droplets, they can be separated by rather sophisticated electronics. A further enhancement of this technique are the so-called fluorescence activated cell sorting (FACS) devices, which additionally use a fluorescence signal (of previously labeled) cells.

Thus, nowadays flow cytometry has become a powerful tool for accurate scientific and clinical studies. Up to thousands of cells can be addressed per second. Although professional flow cytometers are highly advanced devices that can often be operated only by specially trained personnel, the basic principle of operation is quite simple. Hydrodynamic focusing relies on a converging flow that extrudes the cell suspension along narrowing streamlines. This can also be implemented on microfluidic and lab-on-a-chip devices, to provide solutions for cell sorting and cell separation for new types of applications, where only rather small amounts of liquid are handled and automated analysis is of importance. A lab-on-chip system can easily be integrated into a compact microscopy or fluorescence reader setup. This renders it particularly interesting for point-of-care applications: a portable diagnostic systems is designed to consist of two parts, a (disposable) lab-on-chip, microfluidic system and a processing unit with integrated analysis, such as the lab-on-CD (Riegger 2006). The functionality of the microfluidic solution on a chip certainly must lack the powerful active controls of a laboratory scale flow cytometer, as it is designed to work passively. However, many useful tasks could be carried out such as pre-concentrating cells or identifying coarse anomalies of the blood count.

A promising microfluidic concept for sorting cells is based on the so-called pinched flow-field fractionation. It consists of two steps: the first is similar to the hydrodynamic focusing in flow cytometry: the fluid stream carrying cells is focused, but in addition pinched against the wall of a microfluidic channel. In this way, cells are forced to line up and flow in a sheet or train very close to the wall such that their size determines how far from the wall their center of mass is placed. The second element is the fractionation of the flow field. Various outlet channels connect to the main channel with cells aligned to the wall. Fluidic resistances are designed such that particles of different sizes are sorted by branching the (virtual) streamlines they follow into different outlet channels. Yamada et al. (2004), Yamada and Seki (2005, 2006) and Takagi et al. (2005) and others were able to show that, in principle, a remarkably high separation efficiency could be achieved. Their work seems to indicate though, that a rather elaborate design is required together with careful fabrication. In principle, cell separation by pinched flow-field fractionation can be accomplished with a very simple design. In this work, we explore the minimal design necessary for building a cell sorter for leukocyte pre-concentration, experimentally as well as with simulation techniques. We fabricate and analyze two different layouts, each comprising a rather short pinch region for cell alignment, immediately followed by two outlets separating off red and white blood cells, see Fig. 1 for a schematic picture. The channel dimensions are rather large throughout to avoid clogging (e.g., by air bubbles, when priming the device with isotonic NaCl solution), to enhance throughput, but also to allow for a variety of fabrication technologies: such a device will almost certainly be designed to be disposable; a rather cheap and simple fabrication technique is called for. Although we can show that the use of such a reduced and robust design is very promising, we find that the hydrodynamic analysis of the device with respect to possible optimization is rather difficult. In particular, the ideal

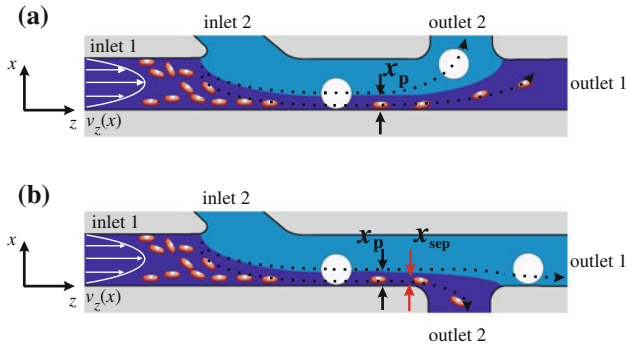

Fig. 1 Hydrodynamic cell sorter used to separate leukocytes (*white spheres*) and erythrocytes (*red plates*). **a** Design 1 and **b** design 2. In a first step, all cells are aligned to the wall by focusing the stream through inlet 1 to a width x_p. The final position of the center of mass relative to the distribution of streamlines close to the outlets depends on the size (and orientation) of the particles but also how they are oriented during the pinch. Many of the erythrocytes may be contained in a flow corridor of width x_{sep} smaller than x_p. Setting the amount of liquid leaving through outlet 2 in **b** (for instance) appropriately can be used to specifically redirect this flow corridor to outlet 2 (color figure online)

dimensioning based on calculating flow rates and determining the direction of streamlines must be supplemented by further aspects that hinge on the explicit dynamics of RBCs in a certain flow geometry. For instance, several hydrodynamic effects originating from the finite extension of the cells and the proximity to a channel wall can lead to the so-called lift forces and to migration across streamlines (Tokarev et al. 2011; Di Carlo et al. 2007).

A series of approaches have been proposed to represent this complicated fluid dynamics problem numerically, whereby the response of the flow field on a dynamically varying shape of an immersed object must be accounted for. Pozrikidis (2003) has studied RBC membrane deformations with a semi-analytical model, whereas Liu and Liu (2006) have carried out a challenging finite-element-analysis of a stack of RBCs in fluid flow. Some of the problems in meshing this fluid dynamics problems can be overcome by stochastic-mesoscopic descriptions (Sun et al. 2003) or off-lattice models (Noguchi and Gompper 2005), allowing to represent drastically changing cell shapes as well. In this respect, fluid particle models are particularly promising, as they allow for a rather simple implementation within Molecular Dynamics schemes and at the same time are sufficiently versatile to represent complex situations involving solid boundaries, fluid flow and advected objects "under one wing". Yuen and co-workers studied columnar stacking of RBCs, employing a fairly detailed representation of all relevant objects (Boryczko et al. 2003a, 2004). Recently, a hybrid approach using a grid representation of the membrane and a fluid particle representation of the blood plasma has been suggested (Fedosov et al. 2010a, b) that allows to represent the interplay of bending rigidity, shape deformation fluid flow on the adhesion dynamics of a RBC to the cell wall. In our case, we have to search for a compromise between detail of description and the required extent of system to be simulated. For this reason, we shall employ the dissipative particle dynamics (DPD) in the spirit as presented by Steiner et al. (2009).

This work is organized as follows. In Sect. 2, the basic design and work principle as well as a classical dimensioning are introduced, assuming that cells can be treated as point-like objects following definite streamlines. Subsequently, in Sect. 3, the technology used for manufacturing the microfluidic structures as well as the experimental setup is presented. Section 4 summarizes the experimental results on cell separation that are in turn further elucidated by a simulation analysis based on the DPD approach. In Sect. 5, we briefly discuss possible hydrodynamic forces that could lead to migration across streamlines and their influence on the characteristics of the sorter.

2 Dimensioning of the cell sorter

Figure 1a illustrates the device geometry and operating principle of the particle sorter. The incoming, cell-laden fluid stream through inlet 1 is pinched along the channel wall. If one approximately thinks of all cells following a definite streamline with their center of masses, one sees that the spherically shaped leukocytes with the smallest radius $\geq$3.5 μm (lymphocytes, cmp. Table 3) must leave their original streamline emanating from inlet 1 and now follow a different one belonging to the stream of inlet 2 if the stream from inlet 1 can be focused up to a distance $x_p < 3.5$ μm from the channel wall. This way, the cells can be sorted through the branching outlets. The ratio of leukocyte enrichment (separation efficiency) is defined as:

$$E = \frac{\text{Concentration of extracted target cells}}{\text{Initial concentration of target cells}}, \quad (1)$$

which should be larger than unity ($E > 1$), since a concentration of the target cells is desired. A high separation efficiency requires an accurate dimensioning which means that the streamlines of the target cells leave the device through outlet 2, while smaller erythrocytes leave the system (due to their small vertical extension) through outlet 1, see Fig. 1a for design 1. If the erythrocytes align parallel to the wall such that their center of mass is very close to it ($\approx$1 μm), then one can achieve a clear distinction between red and white blood cells. The dimensioning of the design can then be accomplished, for instance, with equal flow rates I_1 in inlet 1 and outlet 1 (as indicated by the color scheme in Fig. 1), and I_2 set accordingly to achieve the

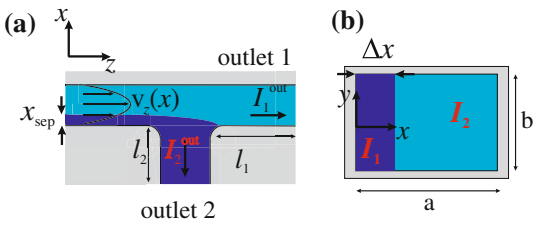

Fig. 2 Illustration of the dimensioning of the separation. **a** *Top view* of device 2 at the branching point. The volume currents I_1^{out} and I_2^{out} determine the dividing plane located at x_{sep} away from the position of the wall. The volume currents can be adjusted by the fluidic resistances of each outlet channel determined by their lengths l_1,l_2. **b** Cross-sectional view of a straight rectangular duct with height b and width a carrying volume currents I_1 within the focused fluid sheet and I_2 within the bulk stream, respectively

desired thickness x_p of the focused stream. This is of course an idealized situation in which x_p would have to be as small as at least 2 μm [the minimal vertical extension of an erythrocyte (Yamada and Seki 2005)]. As we will see, in practice, this is not feasible, and a somewhat larger x_p has to be allowed for. However, as it will turn out, the erythrocytes still have the tendency to align flatly against the channel wall, and in order to sort particles according to their size, it is then sufficient to branch the right amount of liquid into each outlet channel, in Fig. 1, the actual path of a red blood cell is indicated. In this way, the flow through outlet 1 (design 1, a) or outlet 2 (design 2, b) to sort off erythrocytes can be set according to a suitable separation distance x_{sep} (see Fig. 2) in order to keep the clear distinction between the two cell types.

In general, the width of a fluid sheet of thickness Δx parallel to the walls of a straight rectangular channel is determined by the ratio of flow rates belonging to the liquid carried in the sheet and the remaining volume (see cross-sectional view in Fig. 2b). The desired value for Δx can be computed by integrating the flow profile $v_z(x, y)$ over an appropriate area in x and y. The three-dimensional velocity field $v_z(x, y)$ of a fully developed flow in a rectangular duct is given by

$$v_z(x,y) = \frac{4a^2\nabla p}{\eta\pi^3} \sum_{i=1,3,\ldots} (-1)^{\frac{i}{2}} \times \left[1 - \frac{\cosh(i\pi y/a)}{\cosh(i\pi b/2a)}\right] \frac{\cos(i\pi x/a)}{i^3}, \tag{2}$$

where a and b are defined as in Fig. 2b, ∇p is the applied pressure gradient and η is the viscosity. The volume flow rate within the fluid sheet is then

$$I_1 = \int_0^{\Delta x} v_z(x,y)\,\mathrm{d}x\mathrm{d}y, \tag{3}$$

and the volume flow rate of the "bulk" part

$$I_2 = \int_{\Delta x}^{a} v_z(x,y)\,\mathrm{d}x\mathrm{d}y, \tag{4}$$

where $\Delta x = x_p$ or $\Delta x = x_{sep}.x_p$ is determined by the inlet flow rates I_1^{in} and I_2^{in}, and is here determined by flow boundary conditions realized by syringe pumps. At the outlets, we make use of the fact that the volume current flow rates are inversely proportional to the fluidic resistances R_i of each outlet channel,

$$\frac{I_1^{out}}{I_2^{out}} = \frac{R_2}{R_1}. \tag{5}$$

In this way, x_p and x_{sep} can be set independently. For straight channels of the same shape, i.e., $a_1 = a_2$ and $b_1 = b_2$, Eq. (5) reduces to the simple expression

$$\frac{I_1^{out}}{I_2^{out}} = \frac{l_2}{l_1}. \tag{6}$$

For practical reasons, i.e., in order to establish short fluidic connections, the outlet channels (and also the connecting channels) have no uniform cross section along the channel axis. In this case, the dimensioning can be achieved by applying Eq. (5), with R_1 and R_2 obtained from a piecewise summation of resistances of channel segments with uniform cross section.

3 Technology and fabrication

The manufacturing technology used in this work is a variation of the rapid prototyping technique established by Brenner (2005) and will briefly be reviewed here. The fabrication technology can be divided into two basic steps: (i) fabrication of a SU-8 master and (ii) casting of the microchip with a polymer called poly-dimethyl-siloxan (PDMS). The process chain used to manufacture the PDMS chip starts with the fabrication of a replication master. The typical dimensions realized in this work are $d = 30$ μm as channel width and $h = 30$ μm as channel height. An aspect ratio of 1 can easily be realized with SU-8 resist.

The molding master is subsequently used for the molding process as illustrated in Fig. 3. As a first step, the PDMS is casted over the molding master and afterwards the system is degassed in order to avoid air bubbles. In a second step, the casting mould is cured at 70 °C for approximately 4 h. For further details of this process steps, the reader is referred to Brenner (2005). The cured PDMS structure is subsequently removed from the molding cast. In order to establish a fluidic connection, holes are punched through the PDMS chip. Finally, the open channels are

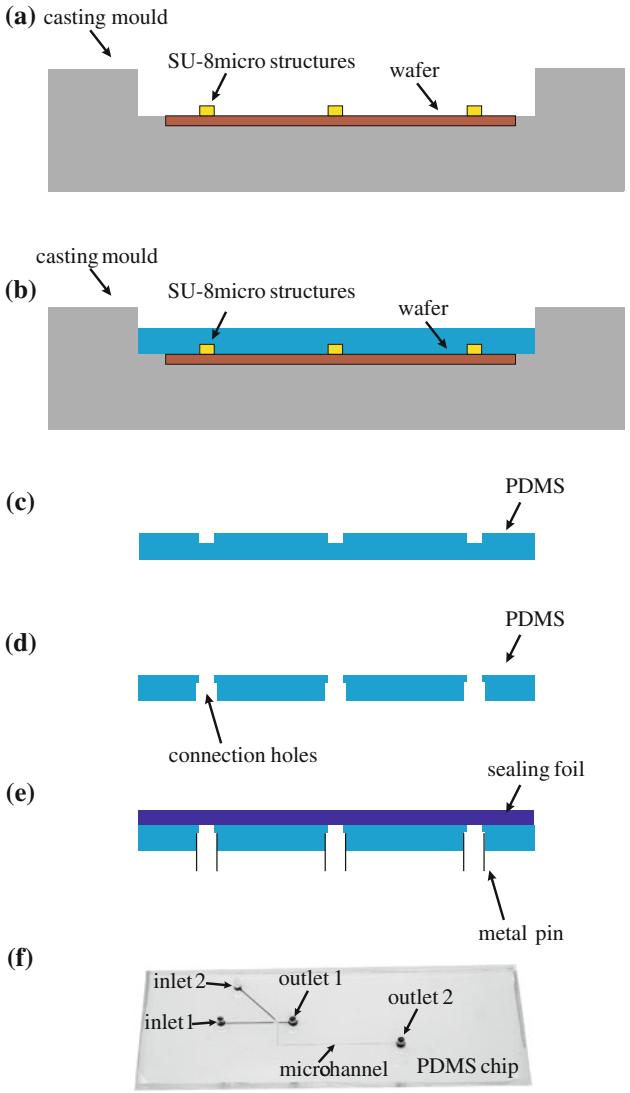

Fig. 3 Process chain of the molding process. **a** The molding master is placed into the molding cast. **b** The PDMS is casted over the molding master and the system is degassed. **c** After curing the PDMS, the PDMS chip is removed from the molding cast. **d** The chip is connected through punch holes before the chip is finally sealed as illustrated in **e**. **f** The PDMS microchip with two inlets, the focusing region of the device and the two outlets, whereas all fluidic connections are realized by metal pins

sealed by a pealing foil as illustrated in Fig 3e, where metal pins are used to connect the chip through the punch holes. Figure 3f shows the PDMS chip with its microchannels, which can easily be accessed by the punch holes. The advantage of the technology used here, is that the dimensioning of the chip can easily be modified by varying the position of the punch holes at the outlet channels. The outer dimensions of the PDMS chip correspond to those of a standard cover slip making it very easy to integrate the chip into an experimental setup using a microscope for visualizing the cells.

4 Experiments and explicit fluid dynamics simulation with dissipative particle dynamics

Before characterizing the behavior of the particle sorter with blood cells, the handling of the microchip and the correctness of the dimensioning were tested using a multiphase flow, i.e., water and a water–ink mixture. Figure 4 shows pictures of the hydrodynamic focusing for different inlet flow rates. With increasing flow rate through the upper channel, the ink phase is squeezed into a fluid sheet of decreasing width. Analytically, the interface position can be calculated in complete analogy to the equations described in Sect. 2. Figure 4d shows the interface position measured in comparison to the analytical calculation, i.e., Eq. (5), over the ratio of inlet flow rates. The numerical model and the experimental data agree quantitatively. For separation experiments with blood cells, human blood tenfold diluted with isotonic NaCl solution enters inlet 1; pure isotonic NaCl solution which enters inlet 2 (the pinching fluid stream) has been employed. The ideal dimensioning would imply a flow ratio of 1:68 at the inlets (with a corresponding ratio at the outlets) to achieve an $x_p = x_{sep} = 2$ µm. During testing of the device, however, it became clear that applying this ratio at the inlets almost completely suppresses the entry of blood cells into the pinch region. This we attribute to an increased crowding of erythrocytes at the inlet that is hard to relieve if the net flow rate through inlet 1 is too small. By systematically increasing the flow rate at inlet 1 relative to inlet 2, we find that a ratio of $\simeq$1:16 (leading to an $x_p \simeq 3.5$ µm, cmp. Fig. 4) is sufficient for a stable and continuous operation. However, according to Fig. 4, this would imply the risk of directing a fraction of lymphocytes to the wrong outlet. At the same time, many erythrocytes still appear to align rather flatly and tightly against the channel wall (e.g., see Fig. 6) and can possibly be skimmed from a smaller flow corridor [a strategy that has been previously explored with respect to hydrodynamic filtering (Yamada and Seki 2005)]. As we shall see, keeping a ratio of flow rates between 1:60 and 1:68, (leading to an $x_{sep} \simeq 2$ µm) at the outlets does not substantially influence the separation efficiency, and the clear distinction between erythrocytes and leukocytes can be kept. In Fig. 5, we show the distribution of streamlines inferred from a CFD simulation, belonging to the ratios of flow rates quoted above that lead to $x_p \simeq 3.5$ µm and $x_{sep} \simeq 2.$ µm. This means that *spherical* particles with radius larger than 2 µm should be separated off safely, a significant fraction of the plasma flow from inlet 1 also enters outlet 2 (design 1) or outlet 1 (design 2).

In the experiment, the operation of the device is monitored by video microscopy tracking single cells. The CCD

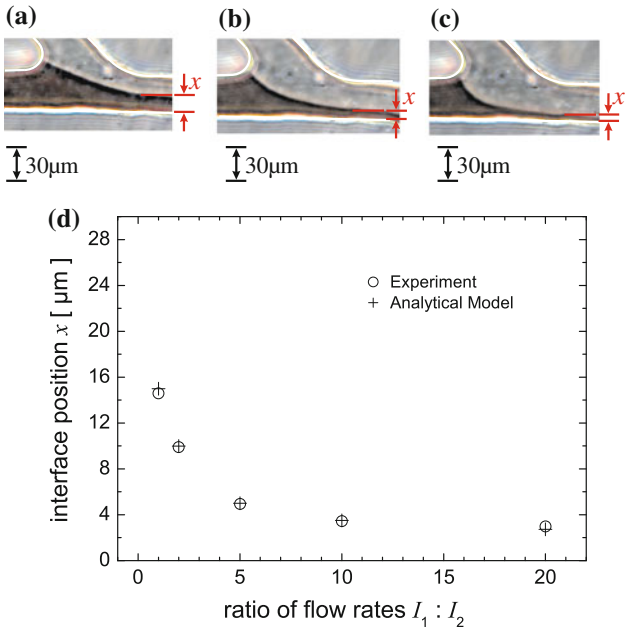

Fig. 4 Hydrodynamic focusing for different inlet flow rates. **a** A flow rate ratio of 1:1, **b** 1:5 and **c** 1:10. **d** Interface position between water–ink mixture and water for hydrodynamically focused flow in dependency of the ratio of flow rates

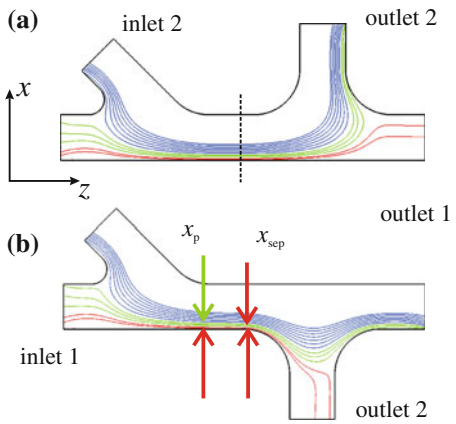

Fig. 5 Distribution of streamlines for design 1 (**a**) and design 2 (**b**), computed from a CFD-simulation with flow boundary conditions, and the actual 3D geometry of the devices, with square cross sections. The ratio of flow rates I_1^{in}:I_2^{in} at the inlets has been set to 1:16 (**a**, **b**), and I_1^{out}:I_2^{out} to 1:68 at the outlets in (**a**), and 68:1 in (**b**). The streamlines have been generated by choosing starting points along the x direction in the middle of channel (*dashed vertical line*), perpendicular to the y direction (pointing into the paper plane), and integrating the trajectories towards inlets and outlets. The ensemble of streamlines is, to a good approximation, contained in single plane (parallel to the plane of the paper) (color figure online)

camera has a maximum rate of 200 pics/s, capturing an area as large as the one shown in Fig. 6. This figure also indicates that leukocytes can be distinguished well from red blood cells, as they appear larger and brighter and as almost perfectly spherical. Furthermore, due to the scarce

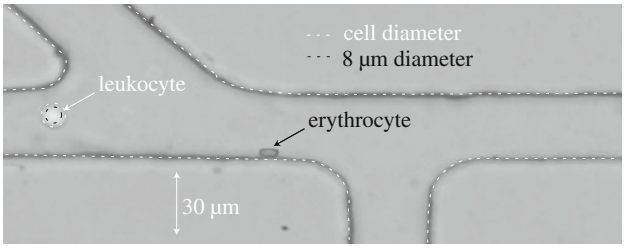

Fig. 6 Human leukocyte and erythrocyte in the microfluidic particle sorter. The *white dashed line* indicates the contour of the leukocyte as estimated from the photograph (diameter 11.3 µm), while the *black dashed line* marks a diameter of 8 µm

occurrence of leukocytes, the path of each one passing the device region can uniquely be identified, although average flow velocities are of the order of cm/s and a single cell passes the pinch region within a fraction of a second. For the red blood cells, owing to their higher concentration, one must be more careful, and we proceeded as follows. A total of 1,000 successive erythrocytes were selected when entering the pinch region through inlet 1. If their path could uniquely be identified to lead to either outlet 1 or 2, the cell was included in the statistics. In this way, we could keep 200 reliable paths. Not only insufficient temporal resolution or contrast invalidates the initially chosen erythrocyte, but also the fact that the flow pattern is actually three-dimensional, which means that the RBCs may only partially meet the focal plane. For the same reason, a more detailed analysis of single RBC with respect to changes in orientation is not feasible. It is therefore difficult to assess in how far the picture of cells following definite streamlines really applies, especially when RBCs temporarily crowd at inlet 1.

To gain further insight into the functioning of the cell sorter as described above, we employ a numerical approach with an explicit simulation of extended flexible objects in fluid flow. As most standard CFD software packages are unable to deal with this problem, we decided to model the fluid dynamics in the pinched flow region within the DPD framework, where the dynamics of the fluid and of suspended objects can be represented in a unified manner by soft interacting point particles (Groot and Warren 1997), the dynamics of which follows Newton's second law with a force $\mathbf{F}_i = \sum_j (\mathbf{F}_{ij}^{C} + \mathbf{F}_{ij}^{D} + \mathbf{F}_{ij}^{R}) + \mathbf{F}_i^{ext}$ acting on particle i with mass m_i. $\mathbf{F}^{C}$ is a conservative force, $\mathbf{F}_{ij}^{C} = A_{ij} w^{C}(r_{ij}) \mathbf{e}_{ij}$, $\mathbf{r}_{ij} = \mathbf{r}_i - \mathbf{r}_j$ is the inter-particle vector, $r_{ij} = |\mathbf{r}_{ij}|$ and $\mathbf{e}_{ij} = \mathbf{r}_{ij}/r_{ij}$. The weight function $w^{C}(r) = (1 - r/r_c)$ vanishes for r_{ij} larger than a cutoff radius r_c and determines the effective range of forces. r_c is conveniently taken as the unit of length, and is commonly set to unity ($r_c = 1$). $\mathbf{F}_i^{ext}$ is an (arbitrary) external force acting on particle i. $\mathbf{F}^{ext}$ is typically used to "freeze" particles supposed to form solid boundaries, or to impose restraints on

relative particle motion, such as a harmonic bond. The conservative interaction potential is usually chosen rather soft to allow for a large time step in integrating the equations of motion. When representing a fluid, however, this would give rise to a very low viscosity. The major part of the viscosity is actually provided by the dissipative force $\mathbf{F}_{ij}^{\mathrm{D}}$ (Groot and Warren 1997), $\mathbf{F}_{ij}^{\mathrm{D}} = -\gamma w^{\mathrm{D}}(r_{ij})(\mathbf{v}_{ij} \cdot \mathbf{e}_{ij})\mathbf{e}_{ij}$, in combination with the random force $\mathbf{F}_{ij}^{\mathrm{R}}$ (Marsh et al. 1997), $\mathbf{F}_{ij}^{\mathrm{R}} = \sigma w^{\mathrm{R}}(r_{ij})\xi_{ij}\mathbf{r}_{ij}(\Delta t)^{\frac{1}{2}}, r_{ij} < 1$, both of which vanish for $r_{ij} > 1$. σ is the amplitude of the random variable ξ_{ij}. $\mathbf{v}_{ij} = \mathbf{v}_i - \mathbf{v}_j$ is the relative velocity of two particles. If we set $\sigma^2 = 2\gamma k_{\mathrm{B}}T$ (k_{B} : Boltzmann constant) and $w_{ij}^{\mathrm{R}}(r)^2 = w_{ij}^{\mathrm{D}}(r)$, random and dissipative forces act as a thermostat and define a system temperature. A common procedure is to set $w^{\mathrm{R}} = w^{\mathrm{C}}$ (Español and Warren 1995). The equations of motion may then be solved by a simple modified *Velocity-Verlet* algorithm (Groot and Warren 1997), or improved schemes (Peters 2004; Lowe 1999; Vattulainen et al. 2002).

Many material properties of an ensemble of dissipative particles can be tuned by choosing an appropriate set of constants A_{ij}, such as surface tensions/energies or the compressibility. If particle i is to represent a solid (s) and j a liquid (l), one would assign a single constant A_{sl} to every solid–liquid pair and A_{ll} for interacting liquid particles. We set $A_{\mathrm{sl}} = A_{\mathrm{ll}} = 40.0$, i.e., we have fully wettable surfaces. The solid boundaries are constructed as "living" walls as described in (Henrich et al. 2007; Cupelli et al. 2008). In particular, we keep the same particle density for immobile solid walls and also for mobile extended objects advected with the flow; this helps reducing boundary artifacts (Steiner et al. 2009; Henrich et al. 2007). In a similar way, extended objects such as blood cells are created. They are represented as compound objects made of elementary fluid particles during the simulation by selecting sets of particles within non-overlapping volumes of fluid. For red blood cells, we chose disk-like volumes of height $2r_{\mathrm{c}}$ and diameter $8r_{\mathrm{c}}$. As illustrated in Fig. 7, neighboring particles i and j with the position $\mathbf{r}_i(t)$ and $\mathbf{r}_j(t)$ are connected via harmonic springs, if their distance at the time t_0 of object creation $|\mathbf{r}_i(t_0) - \mathbf{r}_j(t_0)|$ is smaller than a specified interaction radius r_{cl}. The additional spring force between two neighboring particles i and j is simply $\mathbf{F}_{\mathrm{s}} = -k_{\mathrm{s}}[\mathbf{r}_{ij}(t) - \mathbf{r}_{ij}(t_0)]$, k_{s} is set to $k_{\mathrm{s}} = 100.0$, and $r_{\mathrm{cl}} = r_{\mathrm{c}}$. White blood cells were created analogously, as spherical objects of radius $6r_{\mathrm{c}}$ corresponding to a typical diameter of 12 μm, cmp. (Table 3). Our technique of creating blood cells as semi-flexible compound objects is very similar to the approach employed in Boryczko et al. (2003a, b, 2004).

The length scale of the interaction range r_{c} was set to 1 $r_{\mathrm{c}} = 1$ μm. The density of the DPD fluid is set to $5.0/r_{\mathrm{c}}^3$,

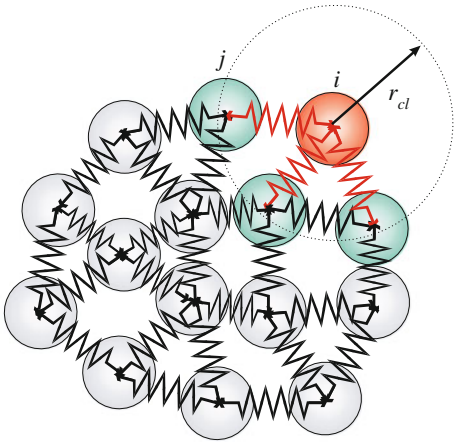

Fig. 7 Schematic picture of the numerical implementation of extended objects. All particles with an initial distance $|\mathbf{r}_{ij}(t_0)| = |\mathbf{r}_i(t_0) - \mathbf{r}_j(t_0)|$ smaller than the cutoff range r_{cl} i.e., $|\mathbf{r}_{ij}(t_0)| < r_{\mathrm{cl}}$, are connected via a harmonic spring

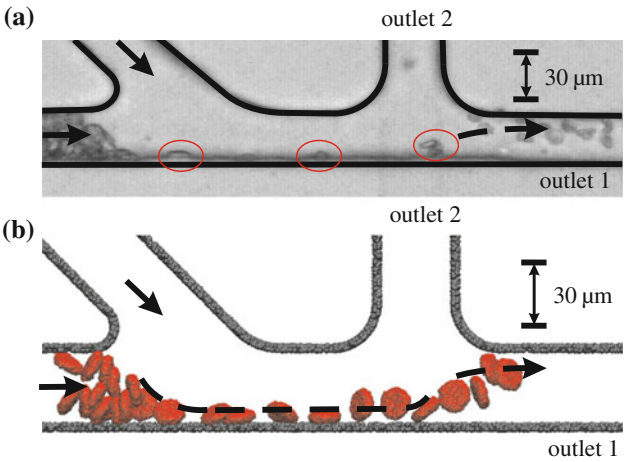

Fig. 8 **a** A snapshot of design 1 in operation. Along the pinch region, three sample erythrocytes have been *encircled* that could uniquely be tracked to end up in outlet 1 (*dashed line*). **b** A corresponding DPD simulation of the flow behavior of blood cells in design 1 at a flow rate ratio 1:16 at the two inlets. As in the experiments, the stream of blood cells is pinched against the channel wall

$\sigma = 5.0$ such that the viscosity in DPD units is $\eta \approx 1.8$ (determined with an auxiliary simulation with Lees–Edwards boundary conditions). With these settings, we can represent the flow problem faithfully with respect to characteristic dimensionless numbers such as the channel Reynolds number ($\simeq 0.4$ at a maximum velocity of 1.4 cm/s), without straining the properties of the DPD fluid too much (for a detailed discussion, see Steiner et al. 2009).

Figure 8a shows a typical photograph of device 1 in operation, in comparison to a corresponding DPD simulation shown in Fig. 8b. The configuration of cells shown in the picture of the simulation is actually three-dimensional, only a thin slice of the channel wall within the plane of the paper

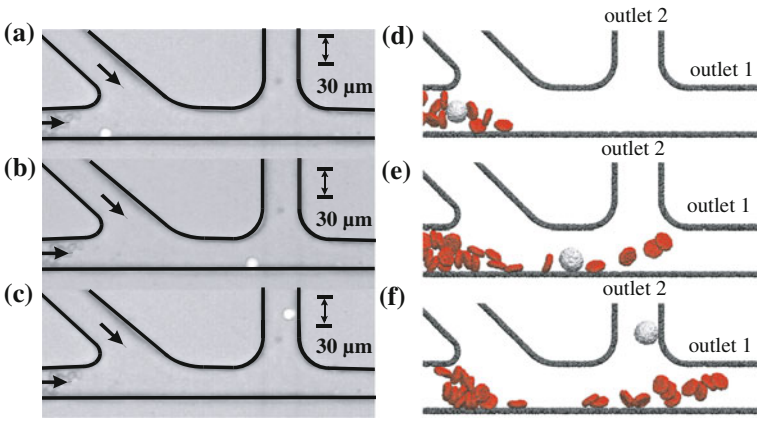

Fig. 9 **a–c** A typical sequence of the flow behavior of a leukocyte entering at inlet 1 and leaving the chip through outlet 2. **d–f** The result of the corresponding DPD simulation. Due to interactions with the channel wall single RBCs are observed to stumble, such as e.g., the cell in the wake of the leukocyte in **e**

has been kept to enhance visibility. The simulation involves a total number of approximately 2.2 *Mio*. fluid particles, including large reservoirs connected to the inlets and outlets. The reservoirs have the same depth (30 r_c) as the channels, but are considerably wider, to allow for sufficient supply of fluid during the simulation. The flow rates have been set by slowly displacing fluid in the reservoirs by pistons, for instance, at velocities of 0.1 (inlet 1) and 1.6 (inlet 2), respectively (DPD units), to arrive at the experimental ratio of flow rates of 1:16 and a corresponding value of $x_p \simeq 3.5\ r_c$. The velocity of the pistons at the outlet reservoirs have been set accordingly, to provide the appropriate ratio of 1:68 for $I_1^{out} : I_2^{out}$ for design 1, for instance. In this way, the whole fluid volume is sealed by wall components: a closed circulatory system to achieve steady state operation is rather awkward to implement, especially with respect to imposing the correct flow boundary conditions. As a consequence, whereas the real device is monitored during continuous operation, the simulation must proceed with a sufficiently large number of RBCs initially situated within inlet 1 (24 RBCs in each simulation). The corresponding crowding of cells at inlet 1 is subsequently relieved as cells are leaving the inlet and pass through the pinch. Under the conditions mentioned above, the simulations to be carried out are quite expensive computationally and the number of runs is limited to a few. With the initial conditions described, we have carried out two runs for design 1 (displayed in Figs. 8, 9) and two for design 2 (Figs. 10, 11). Unfortunately, this is not sufficient for a quantitative comparison between experiment and simulation, but provides valuable insights into the qualitative behavior of cell dynamics in this special flow geometry. For instance, in the experiments, cell crowding at the inlet frequently occurs at the concentrations of blood cells employed in the experiments. This situation, which is rather critical to the behavior of the device, is thus well represented even with a single simulation. In particular, the simulation also shows the "rouleaux" effect. At the time of cell creation during the simulation their orientations are chosen randomly, but after a short initial run time, the

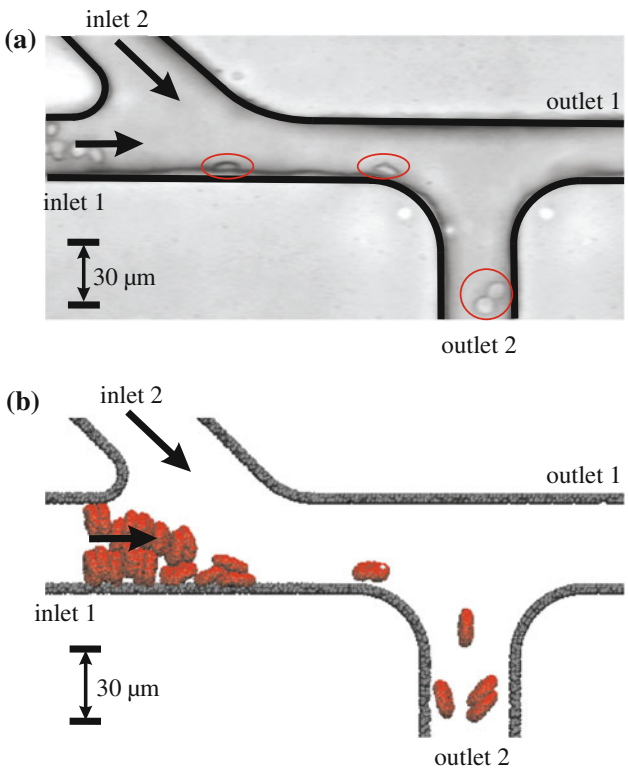

Fig. 10 **a** Flow behavior of blood cells in design 2 at a flow rate ratio 1:16 at the inlets. The stream of blood cells is focused and the erythrocytes are aligned at the wall (marked with *red ellipses*). The blood cells pass the pinch region at a much higher velocity than they travel within their designated outlet (outlet 2). There, flow and shear rates are small, erythrocytes can now reorient such that many of them can be perceived as flat disks (*red circles*). **b** Corresponding DPD simulation under similar flow conditions. A crowded stack of cells is not in general relieved uniformly. The *lower* three erythrocytes arrive in outlet 2 as a bunch before the following two RBCs were released as single cells (color figure online)

crowding erythrocytes show columnar stacking: on average, the long axis of the erythrocytes points perpendicularly to the flow direction (see Figs. 8, 9, 10, 11). This is a well-known phenomenon that has been reported in other studies (Boryczko et al. 2003a).

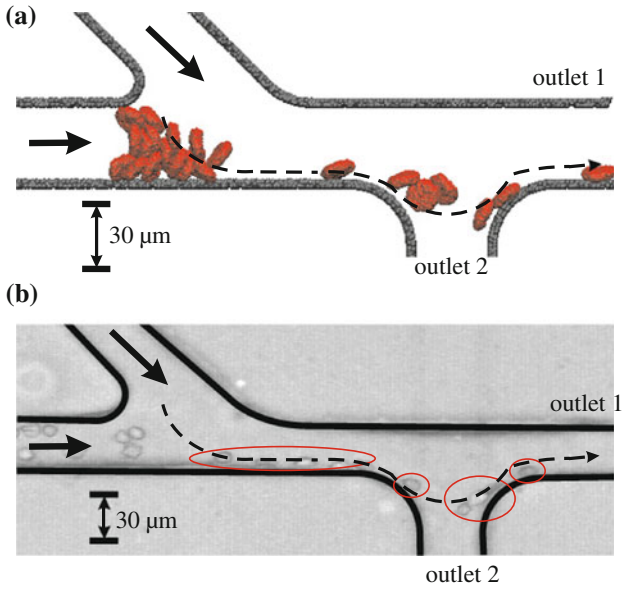

Fig. 11 **a** The behavior of imperfectly aligned erythrocytes in the DPD simulation close to the bifurcation of fluid streams. Boundary conditions as in Fig. 10. **b** An experimental picture of insufficiently aligned erythrocytes that leave the chip through the wrong outlet. From both, **a** and **b**, it may be inferred that the deflection from a streamline leading to outlet 2 is small; before leaving through the wrong outlet, each cell takes a significant excursion downwards, compare also the distribution of streamlines in Fig. 5b. Here, the *dashed lines* are not actual streamlines, but a rough guide to the eye of the cell path

Experimentally, one finds for design 1 that 87 % of the erythrocytes leave the chip through the designated outlet (outlet 1), while in all 47 occurrences of white blood cells traced, these were directed to the correct outlet. For design 2, 69 % of the erythrocytes were sorted into the correct outlet, and all of the 50 observed occurrences of white blood cells recorded along with the experiments with design 2 were directed to the correct outlet. The simulation (see Figs. 8b, 9d–f for design 1, Figs. 10b, 11a for design 2) in general supports these results. Nearly all erythrocytes in these four simulations leave through outlet 1 for design 1 (the correct one) and outlet 2 for design 2, respectively. In the experiments, RBCs apparently align rather flatly against the channel wall (see Figs. 6, 8a, 10a), despite the non-ideal pinch. The corresponding simulations show the same tendency, but here one can infer more clearly that many of erythrocytes retain a slight tilt against the channel wall, a few start tumbling or flipping, especially when they touch the wall or interact with other cells (see Fig. 9, for example). Due to cell crowding (which is slightly overemphasized in the simulations), these aspects become particularly pronounced. Missing a better separation efficiency should then primarily be due to misaligned erythrocytes, that is, those that pass the pinch region with too large a tilt against the channel wall, thereby probing the stream directed to outlet 2 (design 1) or outlet 1 (design 2). Thus, under the experimental conditions given, we should not expect that a nearly perfect (close to 100 %) separation efficiency could be achieved.

It is interesting to observe in the simulation how the redirection occurs in a case when several consecutive cells are traveling very close to the dividing surface of the two outlet streams. Such a situation could indeed be captured in a simulation run for design 2 (see in Fig. 11a). Cells slow down and closely approach the stagnation region of the flow, eventually touch the channel wall before being accelerated toward either outlet. In (**b**), we could track a similar situation in experiment (compare also the approximate location of the stagnation region from Fig. 5b between red and green streamlines) but the detailed dynamics of the cells cannot be resolved. An erythrocyte may thus probe both fluid streams of the bifurcation to outlet 1 and 2 for a relatively long time, and depending on its orientation or dynamics (it may drift at any angle with respect to the streamlines, but also flipping can be observed), various hydrodynamic forces may lift a cell away from the (virtual) streamline it was following and ultimately decide about the final direction. Such lift forces are well known to be effective when suspended particles or cells travel over longer paths (Tokarev et al. 2011; Di Carlo et al. 2007; Segré and Silberberg 1961). In the following, we discuss briefly if and how they could act over rather short distances in a confined geometry.

5 Lift forces acting on cells

The results of the preceding section clearly show that at least for erythrocytes, the idealized picture of cells following streamlines inferred from the "clean" device (operating without cells) is likely to break down. Already the initial erythrocyte alignment in the pinched flow could be due to the result of cells migrating *across* streamlines: although a portion of the volume flow from inlet 1 enters outlet 2 (taking design 1 as an example), the majority of RBCs are collected into the right outlet 1. On the other hand, although the two designs differ only in the vertical direction of outlet 2 (in x direction), design 2 shows a significantly lower separation efficiency.

In the following, we describe some of the hydrodynamic mechanisms that might be relevant to our case. Figure 12 shows a schematic picture of design 2, with streamlines inferred from a CFD simulation of the device without cells. Various types of hydrodynamic forces may act on an erythrocyte during several stages, designated (a)–(c). During (a), the initial focusing of the flow from inlet 1, the cell orientation changes from vertical/tilted to rather horizontal in most of the cases, as also found in Takagi et al.

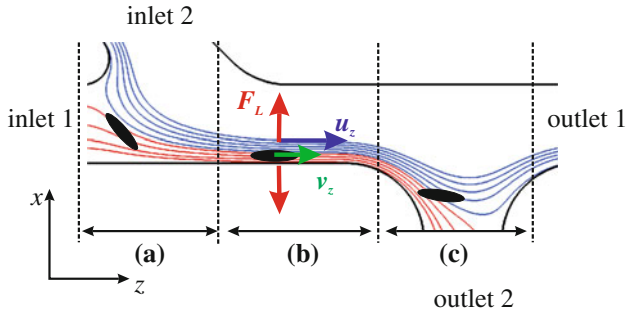

Fig. 12 Illustration of different stages during which forces might act on a cell that lead to streamline migration. The streamlines have been computed from a CFD simulation on design 2, with equal flow ratios at inlets and outlets (1:16), leading to a pinch width of $\simeq$3.5 μm (*red bundle* of streamlines emenating from inlet 1). The *black ellipses* signify the position and orientation of an erythrocyte, that in the pinch region (b) moves with velocity v_z. u_z denotes the local fluid velocity, interpolated from the surrounding flow field to the center of the cell. In (b), when the RBC can hydrodynamically interact with the wall, a lift force F_L of various origins may act on the cell (color figure online)

(2005). In the situation of the crowded inlet, however, the converging flow of the liquid initially accelerates faster than a cell (that is removed from the plug of RBCs) and contributions from inviscid hydrodynamics can be expected: the fluid in the gap between wall and cell accelerates faster leading to a lower pressure and a lift towards the wall (Bernoulli effect) (Zeng et al. 2005). But also in region (b), lift forces (designated as F_L in the figure) due to inertial effects may arise. This is because of the disturbance of the flow field in the presence of an extended object when there is still a notable slip velocity of the advected particle with respect to the surrounding fluid (i.e., a finite $v_s = v_z - u_z$ in Fig. 12) and/or a hydrodynamic interaction with the channel wall. For spherical particles and bubbles, several scenarios have been discussed (Rubinow and Keller 1999; Takemura and Magnaudet 2003; Saffman 1965; Cox and Hsu 1977; Cherukat et al. 1999). Cherukat and McLaughlin (1994) have investigated a case similar to the situation in (b), a solid particle moving in a shear field near a flat wall. We shall use their results to estimate the vertical distance $\delta x(t)$ advanced by a spherical particle of radius $R_0 = 5$ μm within a time t over a distance l (in z direction) with velocity v_z. We can easily demonstrate that the initial (lateral) acceleration of the particle (cell) is relatively unimportant. The equation of motion for δx reads

$$m_P \ddot{\delta x} = -6\pi\eta R_0 \dot{\delta x} + F_L, \tag{7}$$

where acceleration due to F_L is counterbalanced by Stokes drag. Equation (7) can be solved analytically; setting $C = F_L/m_P, C_1 = 6\pi\eta R_0/m_P$, Eq. (7) can be solved by the simple substitution $\delta x(t) = u(t) + t(C/C_1)$, which leads to $\ddot{u}(t) = -C_1\dot{u}(t)$. This is a standard equation, we can solve for $u(t)$ by integrating twice, back substitution then gives

$$\delta x(t) = -\frac{a_1}{C_1}\exp(-C_1 t) + a_2 + t\frac{C}{C_1}, \tag{8}$$

where a_1 and a_2 are integration constants that can be determined from the initial conditions $\delta x(0) = 0$ (at the channel wall) and $\dot{\delta x}(0) = 0$. We immediately see that the exponential vanishes for t larger than a microsecond (with $R_0 = 5$ μm, we have $C_1 = 180{,}000 s^{-1}$), and therefore also the constant $a_2 = -C/C_1^2$ (comprising the result of initial acceleration) is negligible for all practical purposes. So even for the relatively small distance (which we take for convenience as 30 μm) traveled by a particle/blood cell from entering the pinch (a) until it meets the bifurcation (c), we can describe the migration of the particle off the wall by the expression $\delta x(t) = t(C/C_1)$, with the migration velocity $V_{mig} = C/C_1$. We shall now use for F_L the form suggested in Cherukat and McLaughlin (1994):

$$F_L = R_0\eta v_s Re_p I, \tag{9}$$

where $Re_p = R_0 v_s/\nu$ is the particle Reynolds number, $\nu = \eta/\rho = 10^{-6}\mathrm{m}^2/\mathrm{s}$ the kinematic viscosity. The factor I is a function of $Re_p, Re_G = \dot{\gamma}R_0^2/\nu$ and $\kappa = \delta x/R_0$, the ratio of the distance from the wall and the particle radius. The local fluid velocity u_z is defined according to the shear field in the absence of the particle and computed as $u_z = \dot{\gamma}R_0$, where $\dot{\gamma}$ is the shear rate close to the wall. With maximal velocities of the order of cm/s, we may estimate a typical shear rate as $\dot{\gamma} = (1\,\mathrm{cm}/s)/15\,\mu\mathrm{m} = 667\,\mathrm{s}^{-1}$ and $u_z = 0.0033$ m/s. If, for example, we assume that $v_s = -1/2u_z$ (the particle or blood cell is lagging behind of the flow), then $v_z = 1/2u_z$, and the time it takes to travel a distance of 30 μm is $t = 0.02$ s. If we consider a signed Reynolds number for Re_p (depending on the sign of v_s), then $Re_G/Re_p = -2$, and looking up the corresponding tabulated value for I in Cherukat and McLaughlin (1994) is $I = 21.3$, finally yielding

$$C = \frac{F_L}{m_P} = \frac{\rho R_0^2 v_s^2}{m_P} I = 2.77\,\mathrm{m/s}^2, \tag{10}$$

and we have a total "lift" of $\delta x(0.02\ \mathrm{s}) = tC/C_1 = 0.3$ μm. This could be significant if the particle constantly lagged behind; however, as soon as its own velocity becomes comparable to u_z, the lift force becomes very small. A similar calculation at precisely $v_s = 0$ [where we now have to set $Re_p \to Re_G$ (Cherukat and McLaughlin 1994)] would yield $\delta x = 0.05$ μm. In both cases, F_L is directed away from the wall, although under appropriate conditions it can also change sign.

In the above treatment, a rigid spherical object has been assumed; Tokarev (2011) gives an excellent overview of

the different contributions to F_L, especially when cells must be treated as flexible, vesicle-like objects and their dynamics involves deformation or tank treading (Abkarian and Viallat 2008). In these cases, even under creeping flow conditions, lift forces can arise. However, at $Re_p = 0.0165$ (particle lagging behind with half of the local fluid velocity) and/or $\dot{\gamma}$ of the order of 10^3 s^{-1}, the erythrocytes should actually be considered as "solid" (Tokarev et al. 2011), justifying the above analysis for the section (b), and also the DPD model, where RBCs have been treated as semi-flexible objects. Olla (1999) has investigated some consequences of the erythrocytes' ellipsoidal shape on the lift. Most interestingly, he could find a description of how the flipping of RBCs contributes to streamline migration. A steadily flipping red blood cell (given that it can be considered as an oblate ellipsoid) will alternatingly move towards and away from the wall, with a net tendency to move towards the channel axis. This could actually be of significance for erythrocytes entering the bifurcation region, where many of them can indeed be observed to flip. In the simulation, they usually are observed to carry out no more than a half turn.

The precise analysis of the latter issue is for the present geometry also relevant at stage (c), where the flow field first diverges and then bifurcates at a point of stagnation at the channel corner. Here, the finite extension of the cell is important, as it may simultaneously span regions of the flow field that lead to different outlets. The local distribution of pressure and shear gradients probed by the cell (and influenced by it) will then further decide about which outlet is taken. For spherical caps as model cells, this has been investigated by El-Kareh and Secomb (2000); they conclude that for the shape of the object to take effect, they should on average have a common orientation. Experimental investigations have been carried out by Roberts and Olbrich (2003, 2006), especially on the variation of particle separation/deflection for several geometries. They find that for an asymmetrical bifurcation, particles tend to follow the channel segment that was collinear to the segment through which they entered (given the same flow rates throughout). This would, at least qualitatively, correspond to the observation made in our work: in design 2, the erythrocytes would have make a complete right angle turn to separate off correctly, for design 1, the required path is rather straight.

Some final comments must be given on the appropriateness of the DPD method in describing streamline migration correctly. This refers to the stochastic part of the DPD thermostat that inevitably renders any freely suspended object, a Brownian particle. If the compound object considered is sufficiently large and the relevant dynamic time scales small, the diffusive part of the motion can safely be ignored. We shall nevertheless make a rough estimate about how strongly diffusion could make a contribution to, e.g., δx after a distance of 30 r_c has been traversed. Since in the DPD simulation, the slow fluid stream carrying cells is narrowing from 30 r_c thickness to $\simeq 3.5\ r_c$, an increase in average flow velocity from $v_z = 0.1$ (DPD units) to $v_z = 0.86$ must occur in the focused stream. Taking again the above, simplified example of a spherical particle of $R_0 = 5\ r_c$(5 μm) radius, its diffusion constant in the DPD fluid is easily calculated by the Stokes–Einstein relation as $D = k_B T/6\pi\eta R_0 = 6 \times 10^{-3}$[DPD units], and the Péclet number $Pe = v_z l/D$, measuring the relative importance of advection versus diffusion for our case, evaluates as ($l = 30 r_c$) $Pe \approx 4{,}300$. This is significantly larger than 1, a criterion to be met if diffusive transport is to be considered weak. However, the deviation in $\delta x, \Delta\delta x$, when estimated from a mean square displacement, can be as large as $\sqrt{\langle(\Delta\delta x)^2\rangle} = \sqrt{2Dt} = 0.6 r_c$. If situations are to be considered with almost quiescent flow conditions, diffusion effects will be pronounced.

6 Summary and conclusions

In this work, a robust and simple design for a passive hydrodynamic cell sorter for leukocyte enrichment was presented. Two principal designs were investigated experimentally as well as by DPD. For design 1, approximately 87 % of the erythrocytes were collected at the designated outlet (outlet 1), while 100 % (47) leukocytes were sorted to the designated outlet indicating that the function of the chip is limited by the flow behavior of the erythrocytes. For design 2, only approximately 69 % were collected at the desired outlet (outlet 2), while all (50) occurrences of leukocytes were directed to the appropriate outlet. Although video microscopy could be used to characterize the separation efficiency of the two layouts, it was not sufficient to reveal details of the dynamics of the RBCs that could give hints on the mode of device operation. It was only with an explicit simulation of the cell sorter within the framework of DPD that a clearer picture emerges. The video images suggest a rather tight alignment against the channel wall when undergoing the hydrodynamic pinch, although the width of the focused fluid stream has been set to a slightly larger value (3.5 μm) than the vertical extension of the erythrocyte (2 μm). The simulation reveals a general residual misalignment (tilt against the channel wall) of the cells, so a fraction of the cells already enters the wrong fluid stream right after the pinch is completed. That is, for the design and the dimensioning presented, we should expect a non-ideal separation efficiency, although the overall performance as found here can be considered satisfactory, as significant leukocyte enrichment is the main objective here. According to the

discussion in the previous section, additional lift forces in the pinch region (b) should be negligible compared to imperfections in misalignment. For addressing questions such as the difference in separation efficiency between both devices, the stage of bifurcation (c) should be of major concern for further work.

Using DPD models (or similar approaches) along with CFD-based tools in the design process for complicated microfluidic problems could be essential for future case and design studies, especially for applications involving the sorting or manipulation of odd-shaped, flexible and vesicle-like objects, the extension as well as their mutual interaction of which cannot be neglected with respect to the flow field. Although the nature of hydrodynamic forces acting on the cells as discussed in the last section are in principle known, it remains to be elucidated if one can make quantitative use of them to arrive at Eulerian–Langrangian type descriptions of blood cell dynamics that has been developed for macroscopic blood vessels (Worth Longest et al. 2004), and that would facilitate the design for microfluidic cell sorters in general.

Acknowledgments The support of the Deutsche Forschungsgemeinschaft (DFG) for its support within the Priority Program SPP 1164 is gratefully acknowledged.

References

Abkarian M, Viallat A (2008) Vesicles and red blood cells in shear flow. Soft Matter 4:653–657

Boryczko K, Dzwinel W, Yuen DA (2003a) Dynamical clustering of red blood cells in capillary vessels. J Mol Mod 9(1):16–33

Boryczko K, Dzwinel W, Yuen DA (2003b) Clustering revealed in high-resolution simulations and visualization of multi-resolution features in fluid-particle models. Concurr Comput Pract Exp 15(2):101–116

Boryczko K, Dzwinel W, Yuen DA (2004) Modeling fibrin aggregation in blood flow with discrete-particles. Comput Method Prog Bio 75(3):181–194

Brenner T (2005) Polymer fabrication and microfluidic unit operations for medical diagnostics on a rotating disk. Thesis/dissertation. http://urn:nbn:de:bsz:25-opus-23062, http://www.freidok.uni-freiburg.de/volltexte/2306

Cherukat P, McLaughlin JB (1994) The inertial lift on a rigid sphere in a linear shear flow field near a flat wall. J Fluid Mech 263:1–18

Cherukat P, McLaughlin JB, Dandy DS (1999) A computational study of the inertial lift on a sphere in a linear shear flow field. Int J Multiphase Flow 25:15–33

Cox RG, Hsu SK (1977) The lateral migration of solid particles in a laminar flow near a plane. Int J Multiphase Flow 3:201–222

Cupelli C, Henrich B, Glatzel T, Moseler M, Zengerle R, Santer M (2008) Dynamic capillary wetting studied with dissipative particle dynamics. New J Phys 10(4):043009

Di Carlo D, Irimia D, Tompkins RG, Toner M (2007) Continuous inertial focusing, ordering, and separation of particles in microchannels. Proc Natl Acad Sci USA 104(48):18892–18897

El-Kareh AW, Secomb TW (2000) A model for red blood cell motion in bifurcating microvessels. Int J Multiphase Flow 26:1545–1564

Español P, Warren PB (1995) Statistical-mechanics of dissipative particle dynamics. Europhys Lett 30(4):191–196

Fedosov DA, Caswell B, Karniadakis GE (2010a) Systematic coarse-graining of spectrin-level red blood cell models. Comput Method Appl Mech Eng 199:1937–1948

Fedosov DA, Caswell B, Karniadakis GE (2010b) A multiscale red blood cell model with accurate mechanics, rheology and dynamics. Biophys J 98:2215–2225

Groot RD, Warren PB (1997) Dissipative particle dynamics: bridging the gap between atomistic and mesoscopic simulation. J Chem Phys 107(11):4423–4435

Henrich B, Cupelli C, Moseler M, Zengerle R, Santer M (2007) An adhesive DPD wall model for dynamic wetting. Europhys Lett 80(6):60004

Howard M (2003) Shapiro practical flow cytometry, 4th edn. Wiley, New York (Published online 28 Jan 2005)

Liu Y, Liu WK (2006) Rheology of red blood cell aggregation by computer simulation. J Comput Phys 220(1):139–154

Lowe CP (1999) An alternative approach to dissipative particle dynamics. Europhys Lett 47(2):145–151

Marsh CA, Backx G, Ernst MH (1997) Static and dynamic properties of dissipative particle dynamics. Phys Rev E 56(2):1676–1691

Noguchi H, Gompper G (2005) Shape transitions of fluid vesicles and red blood cells in capillary flows. Proc Natl Acad Sci USA 102(40):14159–14164

Olla P (1999) Simplified model for red cell dynamics in small blood vessels. Phys Rev Lett 6(5):453–456

Peters EAJF (2004) Elimination of time step effects in DPD. Europhys Lett 66(3):311–317

Pozrikidis C (2003) Numerical simulation of the flow-induced deformation of red blood cells. Ann Biomed Eng 31:1194–1205

Riegger L et al (2006) Read-out concepts for multiplexed bead-based fluorescence immunoassays on centrifugal microfluidic platforms. Sens Actuators A 126:455–462

Roberts BW, Olbricht WL (2003) Flow-induced particulate separations. AIChE J 49(11):2842–2849

Roberts BW, Olbricht WL (2006) The distribution of freely suspended particles at microfluidic bifurcations. AIChE J 52(1):199–206

Rubinow SI, Keller JB (1999) The transverse force on a spinning sphere moving in a viscous fluid. J Fluid Mech 11:447–459

Saffman PG (1965) The lift on a small sphere in a slow shear flow. J Fluid Mech 22(2):385–400

Segré G, Silberberg A (1961) Radial particle displacements in Poisseuille flow of suspensions. Nature 189:209–210

Steiner T, Cupelli C, Zengerle R, Santer M (2009) Simulation of advanced microfluidic systems with dissipative particle dynamics. Microfluid Nanofluid 7:307–323

Sun C, Migliori C, Munn LL (2003) Red blood cells initiate leukocyte rolling in postcapillary expansions: a lattice boltzmann analysis. Biophys J 85:208–222

Takagi J, Yamada M, Yasuda M, Seki M (2005) Continuous particle separation in a microchannel having asymmetrically arranged multiple branches. Lab Chip 5(7):778–784

Takemura F, Magnaudet J (2003) The transverse force on clean and contaminated bubbles rising near a vertical wall at moderate Reynolds number. J Fluid Mech 495:235–253

Tokarev A, Panasenko G, Ataullakhanov F (2011) Segregation of flowing blood: mathematical description. Math Model Nat Phenom 6(5):281–319

Young B, Lowe JS, Stevens A, Heart JW (2006) Wheater's functional histology, 5th edn. Churchill Livingstone, London

Worth Longest P, Kleinstreuer C, Buchanan JR (2004) Efficient computation of micro-particle dynamics including wall effects. Comput Fluids 33:577–601

Vattulainen I, Karttunen M, Besold G, Polson JM (2002) Integration schemes for dissipative particle dynamics simulations: from softly interacting systems towards hybrid models. J Chem Phys 116(10):3967–3979

Yamada M, Nakashima M, Seki M (2004) Pinched flow fractionation: continuous size separation of particles utilizing a laminar flow profile in a pinched microchannel. Anal Chem 76(18):5465–5471

Yamada M, Seki M (2005) Hydrodynamic filtration for on-chip particle concentration and classification utilizing microfluidics. Lab Chip 5(11):1233–1239

Yamada M, Seki M (2006) Microfluidic particle sorter employing flow splitting and recombining. Anal Chem 78(4):1357–1362

Zeng L, Balachandar S, Fischer P (2005) Wall-induced forces on a rigid sphere at finite Reynolds number. J Fluid Mech 536:1–25